A Mutant Vesicular Stomatitis Virus with Reduced Cytotoxicity and Enhanced Anterograde Trans-synaptic Efficiency

Kunzhang Lin
Huazhong University of Science and Technology https://orcid.org/0000-0001-5091-6197
Xin Zhong
Wuhan Institute of Physics and Mathematics Chinese Academy of Sciences
Min Ying
Wuhan Institute of Physics and Mathematics Chinese Academy of Sciences
Lei Li
Wuhan Institute of Physics and Mathematics Chinese Academy of Sciences
Sijue Tao
Wuhan Institute of Physics and Mathematics Chinese Academy of Sciences
Xutao Zhu
Wuhan Institute of Physics and Mathematics Chinese Academy of Sciences
Xiaobin He (hexb@wipm.ac.cn)
https://orcid.org/0000-0001-8051-130X
Fuqiang Xu
Huazhong University of Science and Technology

Methodology

Keywords: neurotropic virus, output network tracing, vesicular stomatitis virus, attenuated cytotoxicity, enhanced anterograde trans-synaptic tracing

Posted Date: January 23rd, 2020

DOI: https://doi.org/10.21203/rs.2.21708/v1

Version of Record: A version of this preprint was published at Molecular Brain on March 20th, 2020. See the published version at https://doi.org/10.1186/s13041-020-00588-3.

Abstract

Understanding the connecting structure of brain network is the basis to reveal the principle of the brain function and elucidate the mechanism of brain diseases. Trans-synaptic tracing with neurotropic viruses has become one of the most effective technologies to dissect the neural circuits. Although the retrograde trans-synaptic tracing for analyzing the input neural networks with recombinant rabies and pseudorabies virus has been broadly applied in neuroscience, viral tools for analyzing the output neural networks are still lacking. The recombinant vesicular stomatitis virus (VSV) has been used for the mapping of synaptic outputs. However, several drawbacks, including high neurotoxicity and rapid lethality in experimental animals, hinder its application in long-term studies of the structure and function of neural networks. To overcome these limitations, we generated a recombinant VSV with replication-related N gene mutation, VSV-NR7A, and examined its cytotoxicity and efficiency of trans-synaptic spreading. We found that VSV-NR7A exhibits attenuated cytotoxicity, delayed but enhanced anterograde trans-synaptic tracing efficiency, compared with the wild-type VSV. Our work could provide an improved tool for structural and functional studies of neurocircuit.

Introduction

Analyzing the connection of brain neural networks, including input and output neural pathways, is the basis of understanding the mechanisms for brain functions and brain diseases [1, 2]. Trans-synaptic tracing technology based on neurotropic viruses is one of the most effective means to characterize brain neural networks, because viral vectors can be used not only to analyze the structural connections of neural networks, but also to express different genes for functional manipulation [3–11].

The retrograde trans-synaptic tracing systems based on recombinant rabies (RV) and pseudorabies virus (PRV) have been broadly applied for analyzing the input neural networks [3, 12, 13], the use of the anterograde trans-synaptic tracing was limited for the lack of effective viral tools. In retrograde trans-synaptic labeling system, PRV as a trans-multi-synaptic tracer, is widely used in mapping the connection between peripheral-central and central connections [14, 15]. RV, a rigorous trans- mono-synaptic tracer, is broadly used to analyze input brain circuits [4]. Other viral strains or mutants, such as CVS-N2c$^{\Delta G}$, self-inactivated replication deficient rabies virus (SIRV) and G/L gene deletion rabies virus (RV-ΔGL), which can further reduce toxicity, attain long-term gene manipulation for functional studies [6, 13, 16]. In anterograde trans-synaptic labeling system, HSV-1 strain H129 and VSV-Ind are efficient anterograde trans-multi-synaptic tracers for the analysis of output networks [7, 17]. H129, a DNA virus with complex genome, can be used for anterograde multi-trans-synaptic pathways from type-specific starter cells [8]. H129-ΔTK-tdT, with AAV virus complementarily expressing TK, has been reported for anterograde trans-mono-synaptic tracing to visualize direct projections from a specific neuron type [10]. Vesicular stomatitis virus (VSV) has the advantages of simpler structure, higher expression of exogenous genes and wider infection range [7, 18–20]. Envelope glycoprotein of VSV can be replaced by glycoproteins of other viruses to achieve different labeling characteristics and direction controllable trans-synaptic transfer [21, 22]. But these VSVs have high cytotoxicity that can lead to rapid death of mice, which limits long-term

structural observation and gene manipulation or function research, restricting their applications in neuroscience [23]. Several mutants have been obtained by mutating the N gene related to the replication of VSV [24–27]. After mutating the seventh amino acid of the N protein (VSV-N_{R7A}), the replication speed of the virus decreased by 2–3 orders of magnitude within 24 hours [24, 25], which might be used as a better tracer, but whether it still has the ability of anterograde trans-synaptic labeling is still unknown.

Here, we examined the features of VSV-N_{R7A} as an antergrade trans-synaptic tracer. We found that VSV-N_{R7A} exhibits attenuated cytotoxicity, delayed but more efficient anterograde trans-synaptic capability. We conclude that VSV-N_{R7A} can provide longer time window for neural circuits research, making it a possible new tool for the study of brain output networks.

Materials And Methods

Construction of the recombinant mutant VSV vector

pVSV-EGFP was bought from Addgene (plasmid # 36399, Connie Cepko's lab). To construct the mutant VSV (VSV-N_{R7A}), N gene with the seventh amino acid mutation (R to A) was amplified and inserted into the pVSV-EGFP digested by restriction enzyme MscI and BSTZ17I (New England Biolabs). The sequences of primers designed to amplify N mutant were: N'(R7A)-F: tggccaTATGAAAAAAACTAACAGTAATCAAAATGTCTGTTACAGTCAAGGCCATC; N'(R7A)-F1: ATCATTGACAACACAGTCATAG; N'(R7A)-F2: ATGTCTGTTACAGTCAAGGCCATCATTGACAACACAGTCATAG; N'(R7A)-R: gtatacTCAATGTCATCAGGCTGTCGGGCATT. Plasmids were verified by DNA sequencing.

Rescue and preparation of recombinant VSV

Rescue of wild-type VSV (WT-VSV) and mutant VSV (Mutant-VSV) is as previously reported [28]. BHK-21 cells with 6-well plate were incubated with vaccinia carrying T7 RNA polymerase for 1 hour, then washed with PBS three times, and co-transfected with VSV genome plasmid and packaging plasmids encoding the N, P and L proteins in certain proportions. After 6 hours, the supernatant was discarded, and 2 ML Dulbecco's minimum essential media (DMEM) containing 5% fetal bovine serum (FBS) was added to the 6-well plate and cultured in 31 ℃, 5% (v/v) CO2 incubator. After 120 hours, the supernatant was collected and filtered with 0.1 μm filter to infect normal BHK-21 cells. Cells were observed by inverted fluorescence microscopy (Olympus) 24 hours later. The supernatants were collected after complete lesion, filtered with 0.22 μm membrane and centrifuged at 50000× g for 2.5 h at 4 ℃. The precipitation was suspended with PBS and then concentrated and purified with 20% sucrose for the second time. The precipitation was suspended with appropriate amount of PBS. The titer was determined by plaque assay and the virus was stored at -80 ℃.

Single-step growth curves of viruses

Single-step growth curves were carried out at 35 ◦C to determine the replication efficiency of the VSVs. BHK-21 cells were grown in twelve-well plates to a density of 70%~80%, and infected with each recombinant virus at a multiplicity of infection (MOI) of 3. After 1 h of incubation at 35 °C, the viral inoculum was removed, cells were washed 3 times with phosphate buffered saline (PBS), and 1.5 ml of fresh DMEM medium (containing 3% FBS) was added. Supernatants were harvested at different time points (12, 24, 36, 48, 72 and 96 hours post infection (hpi)), and virus titers were detected by plaque assay.

Virus injection and slices preparation

In animal experiments, all surgical and experimental procedures were carried out in accordance with the guidelines formulated by the Animal Care and Use Committee of Wuhan Institute of Physics and Mathematics, Chinese Academy of Sciences, and experiments related to VSV were performed in Biosafety Level-2 （BSL-2） laboratory. Eight-week-old C57BL/6 mice (20-25 g) were used for VSV injection, and injection process was referred to previous study [29]. 0.1 ul 5×10^8 FFU/ml recombinant VSV was injected into VTA and DG area of dorsal hippocampus. The stereotactic coordinates for DG were: AP: -2.00 mm; ML: 1.00 mm; DV: -2.00 mm from the bregma. For VTA were: AP: -3.20 mm; ML: 0.45 mm; DV: -4.30 mm from the bregma. After a certain day, the mice were anesthetized with 5% chloral hydrate (600 mg/kg), and perfused with 0.9% saline and 4% polyformaldehyde solution respectively. Then, the brains were soaked overnight in 4% paraformaldehyde solution. After dehydration was completed with 30% sucrose solution, the brain was sectioned with the thickness of 40 μm by frozen section machine. Brain slices were washed 3 times with PBS, 5 minutes each time. After DAPI staining for 10 minutes, the brain slices were attached to the microscope slides and sealed with 70% glycerol.

Immunohistochemistry and fluorescence imaging

For staining neurons in vivo, the target brain slices were sealed with 10% sheep serum for 1.5 h , and immunostained with a Cy3-conjugated rabbit antibody against NeuN (diluted by PBS at 1:300，Merck Millipore, ABN78C3) overnight at 4℃. For staining microglia cells in vivo, brain slices were blocked with 10% sheep serum in PBS with 0.3% Triton X-100 for 1.5 h, then incubated with primary antibody (anti-Iba1: diluted by PBS at 1:1000, LAK4357, WAKO) overnight at 4°C. After washed 3 times with PBS, slices were incubated with the secondary antibody cy3-conjugated goat anti-rabbit immunoglobulin G (IgG) (1:400, 94600, Jackson) for 1 h at 37°C. All the brain slices above were washed 3 times with PBS, then attached to the microscope slides and sealed with 70% glycerol. Imaging was performed by using the Olympus VS120 Slide Scanner microscope (Olympus).

Results

Mutant-VSV can effectively infect neurons in vivo

Based on the characteristics of rapid amplification, high infection efficiency and expression level of exogenous genes, VSV has been developed into an important gene transfer vector [7, 19]. It has been

previously reported that rearrangement or mutation of viral genes in the genome can reduce the replication speed or toxicity [30-34]. Here, recombinant VSV-N_{R7A} was constructed (Fig. 1). The wild-type and mutant VSV with EGFP reporter were recovered and amplified in BHK21 cells (Fig. 2A). WT-VSV and Mutant-VSV were added to BHK-21 cells at an MOI (multiplicity of infection) of 0.001. When infected with WT-VSV, obvious fluorescence signals can be detected within 12 hours, while Mutant-VSV need 24 hours (Fig. 2B). Significant cytopathic changes were observed after 48 hours in WT-VSV group, however, cytopathies were observed 72 hours later in VSV-N_{R7A} group (Fig. 2B). Compared to WT-VSV, Mutant-VSV exhibit a significant reduction (three orders of magnitude) in virus replication at 35 ℃ within 24 hpi (Fig. 2C), which is consistent with previous findings [24]. In addition, the titer of Mutant-VSV increased with time and reached its peak in 72 hours, which was one order of magnitude less than that of wild-type VSV (Fig. 2C). The ability of the Mutant-VSV to infect neurons in vivo was investigated. The Mutant-VSV was injected into the DG region of mouse brain. The brain slices were prepared at 1 DPI and stained with Cy3-conjugated NeuN antibody. Results showed that EGFP fluorescent signals from Mutant-VSV were co-localized with neurons in vivo (Fig. 2D).

Neuroinflammatory responses induced by the WT-VSV and Mutant-VSV vectors

Viral infections can cause neuroinflammation and induce microglia activation [35, 36]. To evaluate microglial activation induced by WT-VSV and Mutant-VSV infection at the injection site, immunohistochemistry for Iba1, the microglial marker, was performed. As shown in Figure 3, microglial infiltration was markedly increased at the injection site (DG region) following WT-VSV injection, while microglial activation due to Mutant-VSV infection was significantly milder even after 3 days (Fig. 3), indicating that Mutant-VSV is less toxic in the injection site.

Anterograde trans-synaptic labeling with Mutant-VSV vector

VSV has the ability of anterograde trans-synaptic tracing of neural circuits (Fig. 4A), and is used for the output network analysis of specific brain region [37]. To examine anterograde trans-synaptic ability of Mutant-VSV, the Mutant-VSV and WT-VSV were injected into the VTA region of mouse brain, and the brain slices were prepared at 3 DPI and 5 DPI. Green signals were observed in injection site (Fig. 4B). Several brain regions including anterior olfactory nucleus (AON), lateral septal nucleus (LS), nucleus accumbens (ACB), bed nuclei of the stria terminalis (BST), habenula, and dorsal nucleus raphe (DR) were labeled by Mutant-VSV at 3 DPI. However, signals were detected in additional brain regions at 5 DPI, including medial preoptic nucleus (MPN), posterior hypothalamic nucleus (PH), dorsomedial nucleus of the hypothalamus (DMH), periaqueductal gray (PAG), superior central nucleus raphe (CS) (Fig. 4C). These results showed that Mutant-VSV has anterograde trans-synaptic ability, and the trans-synaptic efficiency increases with time. For these brain regions, except MPN, the others are the direct downstream regions of VTA projection according to Allen Mouse Brain Connectivity Atlas (http://connectivity.brain-map.org/). These results suggested that Mutant-VSV may anterogradely label the postsynaptic neurons through one synaptic connection at 3 DPI.

Moreover, more brain regions were labeled by wild-type VSV at 5 DPI, including taenia tecta, dorsal part (TTd), diagonal band nucleus (NDB), olfactory tubercle (OT), caudoputamen (CP), somatosensory areas (SS), globus pallidus, external segment (GPe), substantia innominata (SI), fundus of striatum (FS), magnocellular nucleus (MA), anterior amygdalar area (AAA), anterior hypothalamic nucleus (AHN), central amygdalar nucleus (CEA), basomedial amygdalar nucleus, anterior part (BMAa), retrosplenial area (RSP), parafascicular nucleus (PF), ammon's horn Field CA3 (CA3), temporal association areas (TEa), and piriform area (PIR). These results showed that Mutant-VSV had delayed anterograde trans-synaptic ability (Fig. 4C).

Attenuated lethality of Mutant-VSV in mice brain compared with WT-VSV

Rapid lethality in experimental animals is a limitation for most neurotrophic viruses in neuroscience applications [38]. It is important to determine the survival time of mice infected with neurotrophic virus. Eight-week-old C57BL/6 mice were divided into three groups with 10 mice in each. WT-VSV, Mutant-VSV and PBS were injected intracranially into the DG of hippocampus. WT-VSV was rapidly lethal within 1 week and more than half of the deaths occurred at 4 DPI, which was delayed to 14 DPI in Mutant-VSV group (Fig. 5). The survival percentage was analyzed by Log-rank test ($P < 0.0001$, Fig. 5). These data showed that as compared with WT-VSV, the time of death in Mutant-VSV infected mice was delayed significantly.

More connected brain network were labeled with Mutant-VSV

As the rapid death of experimental animals induced by neurotropic virus, the connected brain networks of injection site was not fully resolved. To determine whether the attenuated virus could label more connected network with the extension of survival time, Mutant-VSV were injected into the VTA of C57BL/6 mice, and the brain slices were imaged at 10 days post-injection. Normal cell morphology of labeled VTA output neurons can be observed at 10 DPI by using Mutant-VSV (Fig. 6A). Moreover, more connected downstream brain regions, which were not labeled at 5 DPI by WT-VSV (Fig. 4C), can be revealed at 10 DPI through Mutant-VSV (Fig. 6B). These results suggested that Mutant-VSV could be used to reveal longer range of downstream networks compared with WT-VSV.

Discussion

Neural network abnormalities can cause many neurological and psychiatric diseases, such as Parkinson's disease, Schizophrenia, Alzheimer's disease and Autism [2]. Analyzing the connection of brain neural networks is the basis of understanding the mechanism of network variation of brain diseases. Mapping brain connectivity networks requires appropriate viral vectors with low toxicity and effective trans-synaptic capabilities, however, the anterograde or retrograde trans-synaptic viruses still need to be improved. Previous studies have reported that VSV can spread anterogradly through multi-trans-synaptic connections in the nervous system and transduce exogenous genes to a variety of organisms, including rodents, invertebrates and non-human primates [20]. This capability of the VSV vectors enables us to express genes of interest in a particular circuit and to analyze the output network. In this study, we

constructed a mutant VSV vector and investigated its characteristics of anterograde trans-synaptic labeling in CNS through the DG and VTA injection in mice. First, the Mutant-VSV can effectively anterograde multi-trans-synaptic spread in vivo, and the trans-synaptic efficiency is related to the time of infection; Second, the Mutant-VSV vector exhibits a smaller degree of tissue inflammation than the wild-type VSV vector, and delayed lethality in mice brain; Third, Mutant-VSV can label more connected downstream network compared with WT-VSV. Thus, the Mutant-VSV vector will be a powerful tool for neuroscientists to investigate the structure and function of a given pathway in rodents or other experimental animals.

In addition to the VSV vectors, the recombinant HSV vectors also permit antetrograde trans-synaptic tracing in the central nervous system [10, 39]. However, as wild-type neurotropic viruses are commonly lethal to experimental animals, the connected brain network of the targeted starter neurons is not fully resolved. In addition, the potential cytotoxicity of these vectors constrains long-term functional experiments. Viral toxicity is mainly related to viral replication, virulent genes and host immune response [27, 40, 41]. The Mutant-VSV vector induces inflammatory responses to a lesser extent than does the WT-VSV vector and slows down the spread of the virus. These properties of the Mutant-VSV vector are ascribable to its replication efficiency, which minimizes adverse side-effects such as inflammatory responses. The slower replication efficiency of Mutant-VSV vector can lead to the delay of trans-synaptic transmission and attenuated lethality in mice brain, which then allows the Mutant-VSV to have more time to label longer range of downstream networks compared with WT-VSV, when injected into the VTA of C57BL/6 mice. Thus, the Mutant-VSV vectors may help researchers to study neuroscience more efficiently and conveniently.

Mutant-VSV can provide a longer time window for neural circuits research, and has the potential to achieve time-dependent anterograde trans-synaptic labeling. For example, Mutant-VSV vector that expresses a slow fluorescent timer (sFT), whose fluorescence color changed from blue to red over time, would enable us to differentiate 2nd-order neurons from 1st-order neurons according to the red-to-blue fluorescence intensity ratio [42]. Moreover, Zheng et al. have reported that neural connections can be detected with ex vivo MRI using a ferritin-encoding VSV, but wild-type viral toxicity affects long-term signal acquisition [11]. Therefore, the Mutant-VSV would be an appropriate vector. However, the Mutant-VSV still have some cytotoxicity. Future studies are required to evaluate functional manipulation of neural circuits with Mutant-VSV carrying optogenetic and calcium indicators, and to develop more low-toxic or even non-toxic VSV vectors.

In summary, our findings suggest that Mutant-VSV (VSV-N_{R7A}) can be used as an efficient anterograde trans-multi-synaptic tracer, with attenuated cytotoxicity, and delayed but enhanced anterograde trans-synaptic spreading. The work can provide a useful new tool for the study of brain output networks.

Abbreviations

VSV: vesicular stomatitis virus; **MOI:** multiplicity of infection; **DMEM:** Dulbecco's minimum essential media; **PBS:** Phosphate buffer saline; **DAPI:** 4',6-diamidino-2-phenylindole; **DG:** Dentate gyrus; **VTA:** Ventral tegmental area; **AON:** Anterior olfactory nucleus; **TTd:** Taenia tecta, dorsal part; **TTv:** Taenia tecta, ventral part; **LS:** Lateral septal nucleus; **ACB:** Nucleus accumbens; **NDB:** Diagonal band nucleus; **OT:** Olfactory tubercle; **CP:** Caudoputamen; **SS:** Somatosensory areas; **MPN:** Medial preoptic nucleus; **BST:** Bed nuclei of the stria terminalis; **GPe:** Globus pallidus, external segment; **SI:** Substantia innominata; **FS:** Fundus of striatum; **MA:** Magnocellular nucleus; **AAA:** Anterior amygdalar area; **Habenula:** Habenula; **AHN:** Anterior hypothalamic nucleus; **CEA:** Central amygdalar nucleus; **BMAa:** Basomedial amygdalar nucleus, anterior part; **AI:** Agranular insular area; **PH:** Posterior hypothalamic nucleus; **DMH:** Dorsomedial nucleus of the hypothalamus; **PF:** Parafascicular nucleus; **RSP:** Retrosplenial area; **TEa:** Temporal association areas; **PIR:** Piriform area; **CA3:** Ammon's horn Field CA3; **DR:** Dorsal nucleus raphe; **PAG:** Periaqueductal gray; **CS:** Superior central nucleus raphe; **HY:** Hypothalamus; **vHPC:** ventral hippocampus; **BLA:** Basolateral amygdalar nucleus; **PFC:** Prefrontal cortex; **ACA:** Anterior cingulate area; **MO:** Somatomotor areas; **SC:** Superior colliculus; **SOC:** Superior olivary complex.

Declarations

Ethics approval and consent to participate

All procedures used were approved by the Animal Care and Use Committees at the Wuhan Institute of Physics and Mathematics, Chinese Academy of Sciences. All the experiments with viruses were performed in Biosafety Level 2 laboratory and animal facilities. Consent to participate: Not applicable.

Consent for publication

Consent for publication: Not applicable.

Availability of data and materials

The datasets used or analysed during the current study are available from the corresponding author on reasonable request.

Competing interests

All authors declare that they have no conflict of interest.

Authors' contributions

KL, XH and FX contributed to the study idea and design; FX and XH contributed to funding acquisition and resources; KL, XZ (Xin Zhong), MY, LL and ST performed the experiments and data acquisition; KL, XZ (Xin Zhong), MY, XZ (Xutao Zhu) and FX accomplished data analysis; KL and FX drafted the manuscript, and contributed to review and editing. All authors read and approved the final manuscript.

Funding

This work was supported by the Strategic Priority Research Program of the Chinese Academy of Sciences (XDB32030200), the Research and Development Program in Key Areas of Guangdong Province (2018B030331001), the Major Research Plan of the National Natural Science Foundation of China (91632303, 31671120), and the National Basic Research Development Program (973 Program) of China (2015CB755601).

Acknowledgements

We thank Lingling Xu from Wuhan Institute of Physics and Mathematics for teaching and guiding confocal imaging.

References

1. Crick F and Jones E. BACKWARDNESS OF HUMAN NEUROANATOMY. Nature. 1993;361(6408):109-110.
2. Insel TR. Rethinking schizophrenia. Nature. 2010;468(7321):187-193.
3. Smith BN, Banfield BW, Smeraski CA, Wilcox CL, Dudek FE, Enquist LW, et al. Pseudorabies virus expressing enhanced green fluorescent protein: A tool for in vitro electrophysiological analysis of transsynaptically labeled neurons in identified central nervous system circuits. Proceedings of the National Academy of Sciences of the United States of America. 2000;97(16):9264-9269.
4. Wickersham IR, Finke S, Conzelmann KK and Callaway EM. Retrograde neuronal tracing with a deletion-mutant rabies virus. Nat Methods. 2007;4(1):47-9.
5. Callaway EM and Luo L. Monosynaptic Circuit Tracing with Glycoprotein-Deleted Rabies Viruses. J Neurosci. 2015;35(24):8979-85.
6. Ciabatti E, Gonzalez-Rueda A, Mariotti L, Morgese F and Tripodi M. Life-Long Genetic and Functional Access to Neural Circuits Using Self-Inactivating Rabies Virus. Cell. 2017;170(2):382-392 e14.
7. Beier KT, Saunders A, Oldenburg IA, Miyamichi K, Akhtar N, Luo LQ, et al. Anterograde or retrograde transsynaptic labeling of CNS neurons with vesicular stomatitis virus vectors. Proceedings of the National Academy of Sciences of the United States of America. 2011;108(37):15414-15419.
8. Lo LC and Anderson DJ. A Cre-Dependent, Anterograde Transsynaptic Viral Tracer for Mapping Output Pathways of Genetically Marked Neurons. Neuron. 2011;72(6):938-950.
9. Beier KT, Borghuis BG, El-Danaf RN, Huberman AD, Demb JB and Cepko CL. Transsynaptic Tracing with Vesicular Stomatitis Virus Reveals Novel Retinal Circuitry. Journal of Neuroscience. 2013;33(1):35-51.
10. Zeng WB, Jiang HF, Gang YD, Song YG, Shen ZZ, Yang H, et al. Anterograde monosynaptic transneuronal tracers derived from herpes simplex virus 1 strain H129. Mol Neurodegener. 2017;12(1):38.

11. Zheng N, Su P, Liu Y, Wang H, Nie B, Fang X, et al. Detection of neural connections with ex vivo MRI using a ferritin-encoding trans-synaptic virus. Neuroimage. 2019;197:133-142.
12. Wickersham IR, Lyon DC, Barnard RJ, Mori T, Finke S, Conzelmann KK, et al. Monosynaptic restriction of transsynaptic tracing from single, genetically targeted neurons. Neuron. 2007;53(5):639-47.
13. Reardon TR, Murray AJ, Turi GF, Wirblich C, Croce KR, Schnell MJ, et al. Rabies Virus CVS-N2c(DeltaG) Strain Enhances Retrograde Synaptic Transfer and Neuronal Viability. Neuron. 2016;89(4):711-24.
14. Sun L, Tang Y, Yan K, Yu J, Zou Y, Xu W, et al. Differences in neurotropism and neurotoxicity among retrograde viral tracers. Mol Neurodegener. 2019;14(1):8.
15. Jia F, Lv P, Miao H, Shi XW, Mei HJ, Li L, et al. Optimization of the Fluorescent Protein Expression Level Based on Pseudorabies Virus Bartha Strain for Neural Circuit Tracing. Frontiers in Neuroanatomy. 2019;13.
16. Chatterjee S, Sullivan HA, MacLennan BJ, Xu R, Hou Y, Lavin TK, et al. Nontoxic, double-deletion-mutant rabies viral vectors for retrograde targeting of projection neurons. Nat Neurosci. 2018;21(4):638-646.
17. Sun N, Cassell MD and Perlman S. Anterograde, transneuronal transport of herpes simplex virus type 1 strain H129 in the murine visual system. Journal of Virology. 1996;70(8):5405-5413.
18. Beier KT, Mundell NA, Pan YA and Cepko CL. Anterograde or Retrograde Transsynaptic Circuit Tracing in Vertebrates with Vesicular Stomatitis Virus Vectors. Curr Protoc Neurosci. 2016;74:1 26 1-27.
19. van den Pol AN, Ozduman K, Wollmann G, Ho WS, Simon I, Yao Y, et al. Viral strategies for studying the brain, including a replication-restricted self-amplifying delta-G vesicular stomatis virus that rapidly expresses transgenes in brain and can generate a multicolor golgi-like expression. J Comp Neurol. 2009;516(6):456-81.
20. Mundell NA, Beier KT, Pan YA, Lapan SW, Goz Ayturk D, Berezovskii VK, et al. Vesicular stomatitis virus enables gene transfer and transsynaptic tracing in a wide range of organisms. J Comp Neurol. 2015;523(11):1639-63.
21. Beier KT, Saunders AB, Oldenburg IA, Sabatini BL and Cepko CL. Vesicular stomatitis virus with the rabies virus glycoprotein directs retrograde transsynaptic transport among neurons in vivo. Front Neural Circuits. 2013;7:11.
22. Hastie E, Cataldi M, Marriott I and Grdzelishvili VZ. Understanding and altering cell tropism of vesicular stomatitis virus. Virus Res. 2013;176(1-2):16-32.
23. Li J, Liu T, Dong Y, Kondoh K and Lu Z. Trans-synaptic Neural Circuit-Tracing with Neurotropic Viruses. Neurosci Bull. 2019;35(5):909-920.
24. Harouaka D and Wertz GW. Second-site mutations selected in transcriptional regulatory sequences compensate for engineered mutations in the vesicular stomatitis virus nucleocapsid protein. J Virol. 2012;86(20):11266-75.
25. Chen L, Yan Q, Lu G, Hu Z, Zhang G, Zhang S, et al. Several residues within the N-terminal arm of vesicular stomatitis virus nucleoprotein play a critical role in protecting viral RNA from nuclease

digestion. Virology. 2015;478:9-17.
26. Chen L, Zhong Y, Hu Z, Qin Y and Chen M. Two second-site mutations compensate the engineered mutation of R7A in vesicular stomatitis virus nucleocapsid protein. Virus Res. 2016;214:59-64.
27. Chen L, Zhou Y, Zhao M and Chen H. R7A mutation in N protein renders temperature sensitive phenotype of VSV by affecting its replication and transcription in vitro. Virus Genes. 2019;55(4):513-519.
28. Whelan SPJ, Ball LA, Barr JN and Wertz GTW. Efficient recovery of infectious vesicular stomatitis virus entirely from cDNA clones. Proceedings of the National Academy of Sciences of the United States of America. 1995;92(18):8388-8392.
29. Zhu X, Lin K, Liu Q, Yue X, Mi H, Huang X, et al. Rabies Virus Pseudotyped with CVS-N2C Glycoprotein as a Powerful Tool for Retrograde Neuronal Network Tracing. Neurosci Bull. 2019.
30. Flanagan EB, Schoeb TR and Wertz GW. Vesicular stomatitis viruses with rearranged genomes have altered invasiveness and neuropathogenesis in mice. J Virol. 2003;77(10):5740-8.
31. Novella IS, Ball LA and Wertz GW. Fitness analyses of vesicular stomatitis strains with rearranged genomes reveal replicative disadvantages. J Virol. 2004;78(18):9837-41.
32. Harouaka D and Wertz GW. Mutations in the C-terminal loop of the nucleocapsid protein affect vesicular stomatitis virus RNA replication and transcription differentially. J Virol. 2009;83(22):11429-39.
33. Kim GN and Kang CY. Matrix protein of VSV New Jersey serotype containing methionine to arginine substitutions at positions 48 and 51 allows near-normal host cell gene expression. Virology. 2007;357(1):41-53.
34. Fang X, Zhang S, Sun X, Li J and Sun T. Evaluation of attenuated VSVs with mutated M or/and G proteins as vaccine vectors. Vaccine. 2012;30(7):1313-21.
35. Chivero ET, Guo ML, Periyasamy P, Liao K, Callen SE and Buch S. HIV-1 Tat Primes and Activates Microglial NLRP3 Inflammasome-Mediated Neuroinflammation. J Neurosci. 2017;37(13):3599-3609.
36. Tanabe S, Uezono S, Tsuge H, Fujiwara M, Miwa M, Kato S, et al. A note on retrograde gene transfer efficiency and inflammatory response of lentiviral vectors pseudotyped with FuG-E vs. FuG-B2 glycoproteins. Sci Rep. 2019;9(1):3567.
37. Zheng Y, Feng S, Zhu X, Jiang W, Wen P, Ye F, et al. Different Subgroups of Cholinergic Neurons in the Basal Forebrain Are Distinctly Innervated by the Olfactory Regions and Activated Differentially in Olfactory Memory Retrieval. Frontiers in Neural Circuits. 2018;12.
38. Ugolini G. Advances in viral transneuronal tracing. J Neurosci Methods. 2010;194(1):2-20.
39. Su P, Ying M, Han Z, Xia J, Jin S, Li Y, et al. High-brightness anterograde transneuronal HSV1 H129 tracer modified using a Trojan horse-like strategy. Molecular Brain. 2020;13(1).
40. David RM and Doherty AT. Viral Vectors: The Road to Reducing Genotoxicity. Toxicol Sci. 2017;155(2):315-325.

41. Liddelow SA, Guttenplan KA, Clarke LE, Bennett FC, Bohlen CJ, Schirmer L, et al. Neurotoxic reactive astrocytes are induced by activated microglia. Nature. 2017;541(7638):481-487.
42. Ohara S, Sota Y, Sato S, Tsutsui KI and Iijima T. Increased transgene expression level of rabies virus vector for transsynaptic tracing. PLoS One. 2017;12(7):e0180960.

Figures

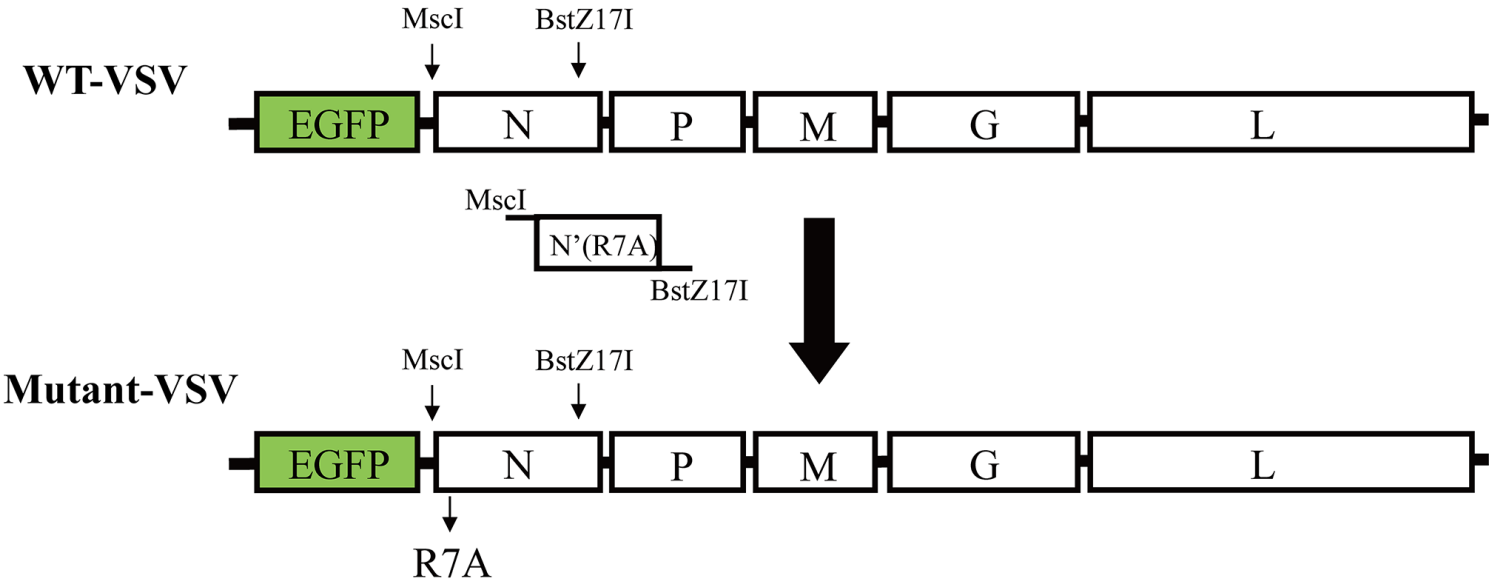

Figure 1

Construction of recombinant VSV with mutant N gene To construct the recombinant mutant VSV vector, N gene with the seventh amino acid mutation (R to A) was amplified and inserted into the pVSV-EGFP digested by restriction enzyme MscI and BSTZ17I.

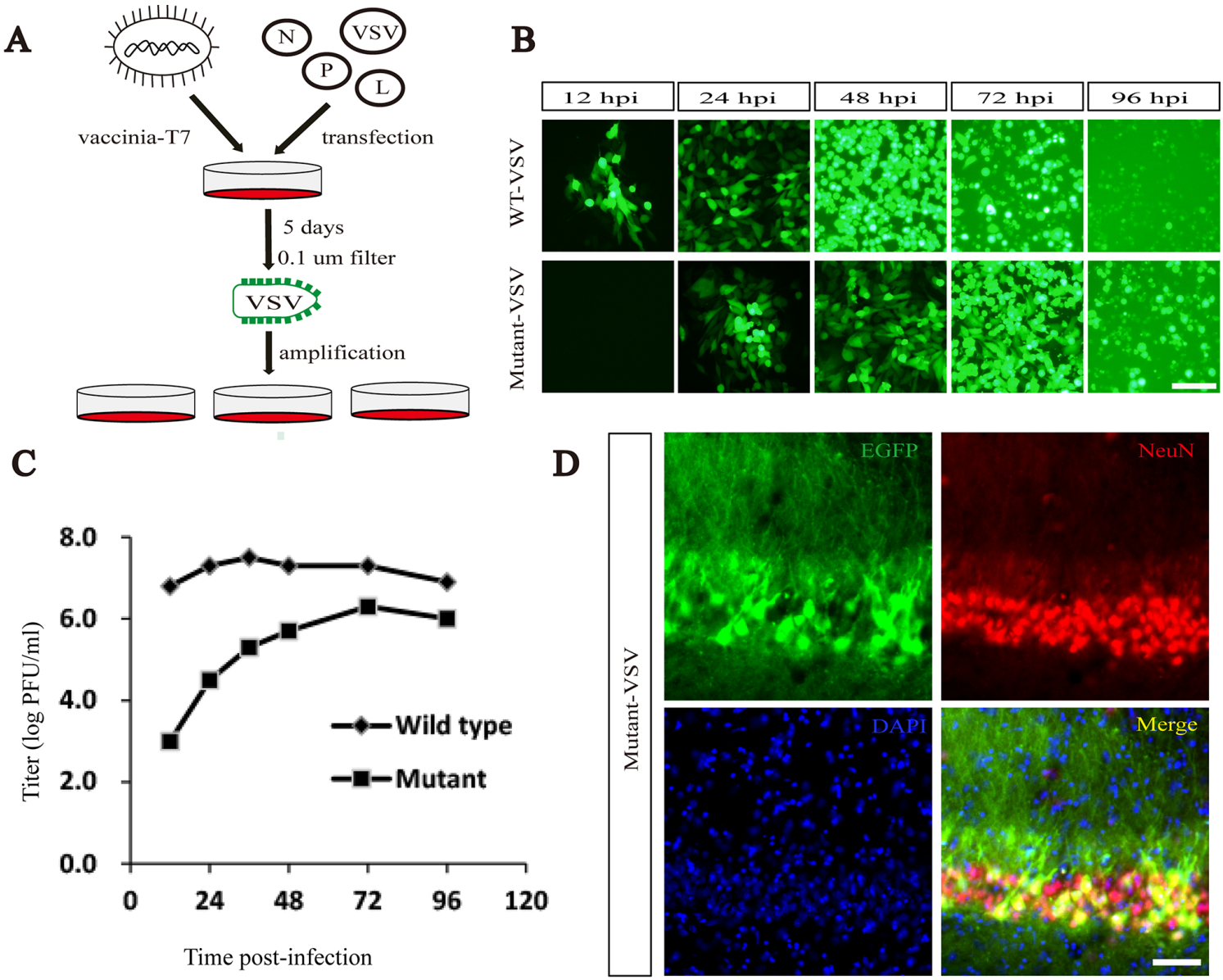

Figure 2

Mutant-VSV effectively infects neurons in vivo (A) Rescue and preparation process of VSV. BHK-21 cells were pretreated with vaccinia carrying T7 RNA polymerase for one hour, then washed with PBS three times, and co-transfected with VSV genome plasmid and packaging plasmids encoding the N, P and L proteins. After 6 hours, they were replaced with fresh culture medium and placed in a 31℃ incubator. 5 days later, the supernatant was collected and filtered with 0.1 μm filter membrane to remove the vaccinia, then added to BHK-21 cells to amplify the VSV. (B) Fluorescent imaging of BHK-21 cells infected with WT-VSV and Mutant-VSV at an MOI of 0.001. When infected with WT-VSV, obvious fluorescence signals can be detected within 12 hours, while Mutant-VSV needs 24 hours. (C) The single-step growth curves of the WT-VSV and Mutant-VSV. The viruses were collected and titered on BHK-21 cells at indicated time points (12, 24, 36, 48, 72 and 96 hpi). (D) Fluorescent signals from mutant VSV were co-localized with neurons in vivo. Cell nuclei were stained using DAPI (blue), neurons were stained with Cy3-conjugated NeuN antibody. Scale bars =100 μm for B and D.

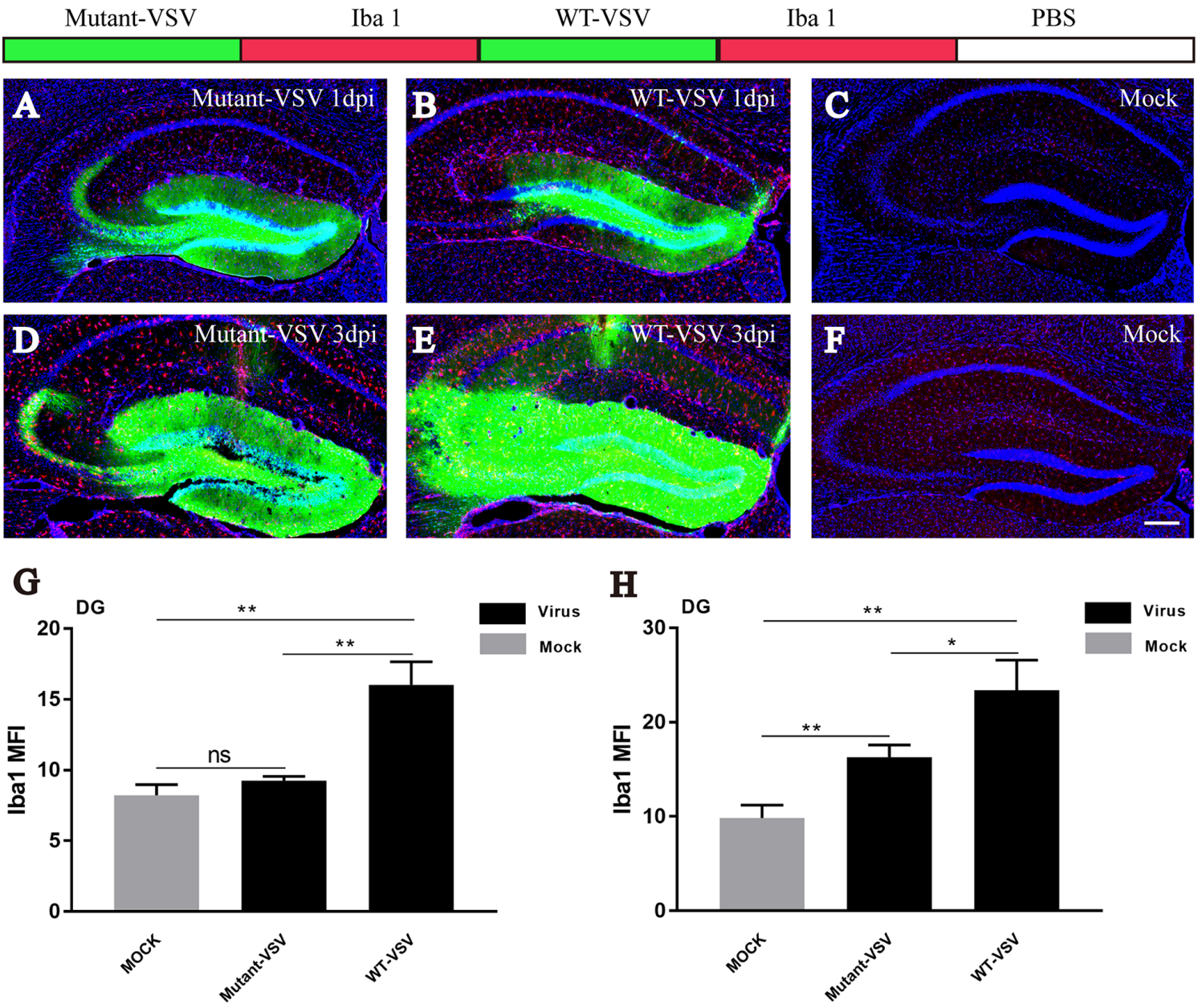

Figure 3

Analysis of inflammatory responses induced by WT-VSV and Mutant-VSV at injection site (A-C) Immunostaining for the microglial marker Iba1 at injection site. Iba1-positive cells were observed in the WT-VSV group at 1 DPI, but barely in the Mutant-VSV or PBS injected (Mock) DG. (D-F) Intense microglial activation was observed at the injection site when WT-VSV or Mutant-VSV was injected into the DG at 3 DPI, and signals in the WT-VSV group were more than that in the Mutant-VSV group, while few signals were observed in the PBS injected (Mock) DG. (G) Quantification of mean fluorescence intensity (Mean ± SEM) of Iba1 in DG at 1 DPI. Mutant-VSV: 9.251 ± 0.182, WT-VSV: 16.02 ± 0.9505, Mock: 8.22 ± 0.4402, Mutant-VSV vs Mock: P = 0.0963; WT-VSV vs Mock: P = 0.0017; WT-VSV vs Mutant-VSV: P = 0.0022; n = 3. (H) Quantification of mean fluorescence intensity (Mean ± SEM) of Iba1 in DG at 3 DPI. Mutant-VSV: 16.29 ± 0.7438, WT-VSV: 23.41 ± 1.836, Mock: 9.828 ± 0.7976, Mutant-VSV vs Mock: P = 0.0041; WT-VSV

vs Mock: P = 0.0025; WT-VSV vs Mutant-VSV: P = 0.0229; n = 3. n is mice number. Scale bars = 200 μm for A-F. Unpaired t-tests, *P < 0.05, **P < 0.01, ***P < 0.001.

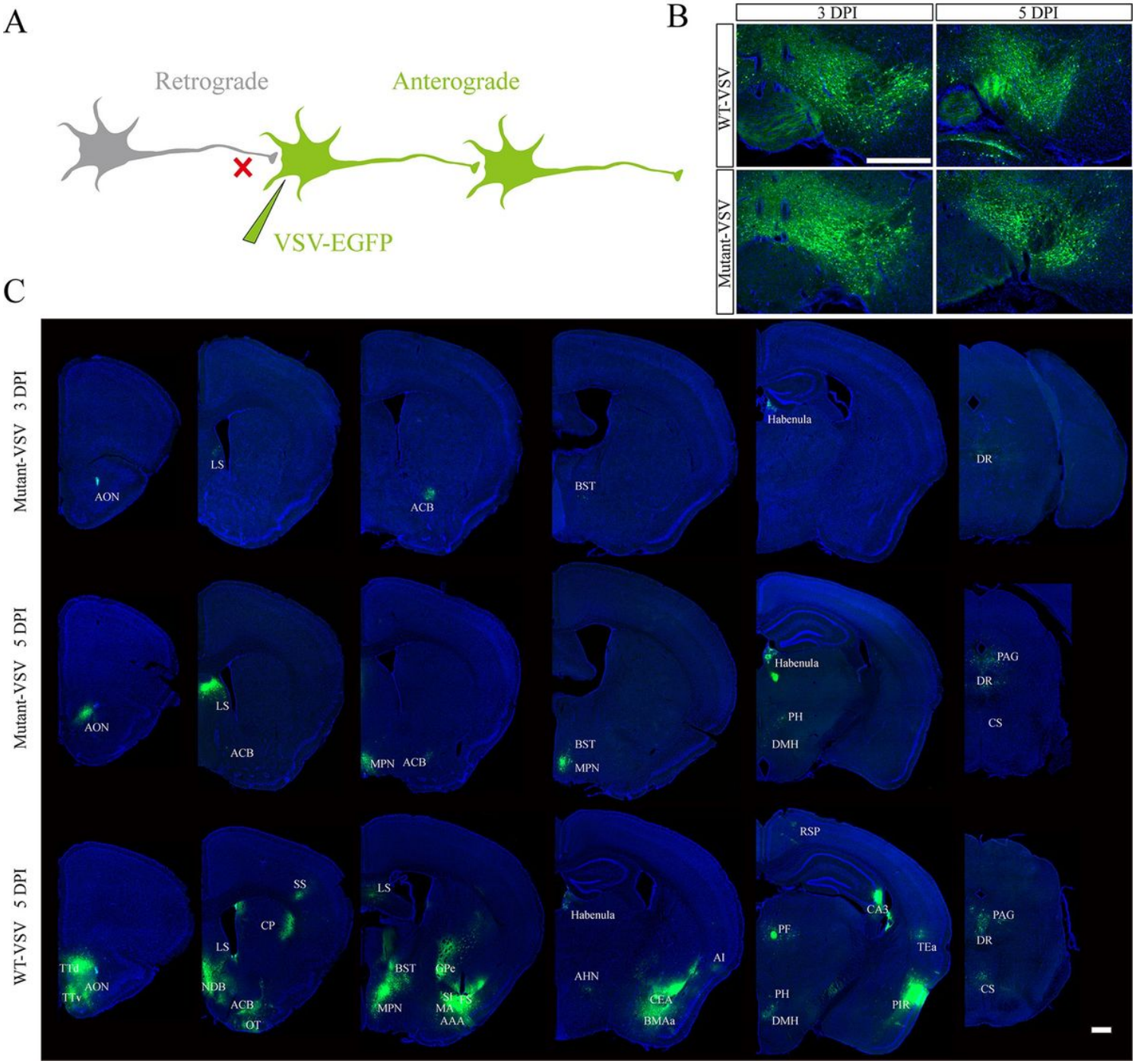

Figure 4

Anterograde trans-synaptic labeling with Mutant-VSV after injection into the VTA (A) Schematic of recombinant VSV anterograde trans-synaptic labeling. (B) The brain slices of injection site at indicated time points (3 DPI and 5 DPI) were imaged. (C) Anterograde trans-synaptic labeling with Mutant-VSV at indicated time points. Mutant VSV can effectively infect downstream brain area of VTA, and more brain regions were labeled over time, but less brain regions were labeled by Mutant-VSV than by WT-VSV at 5 DPI, which showed that Mutant-VSV had delayed anterograde trans-synaptic ability. The EGFP signal was

imaged by using the Olympus VS120 Slide Scanner microscope. Scale bars =500 μm for B and C. The specific name of the brain areas labeled were shown as follows: AON: Anterior olfactory nucleus; TTd: Taenia tecta, dorsal part; TTv: Taenia tecta, ventral part; LS: Lateral septal nucleus; ACB: Nucleus accumbens; NDB: Diagonal band nucleus; OT: Olfactory tubercle; CP: Caudoputamen; SS: Somatosensory areas; MPN: Medial preoptic nucleus; BST: Bed nuclei of the stria terminalis; GPe: Globus pallidus, external segment; SI: Substantia innominata; FS: Fundus of striatum; MA: Magnocellular nucleus; AAA: Anterior amygdalar area; Habenula: Habenula; AHN: Anterior hypothalamic nucleus; CEA: Central amygdalar nucleus; BMAa: Basomedial amygdalar nucleus, anterior part; AI: Agranular insular area; PH: Posterior hypothalamic nucleus; DMH: Dorsomedial nucleus of the hypothalamus; PF: Parafascicular nucleus; RSP: Retrosplenial area; TEa: Temporal association areas; PIR: Piriform area; CA3: Ammon's horn Field CA3; DR: Dorsal nucleus raphe; PAG: Periaqueductal gray; CS: Superior central nucleus raphe.

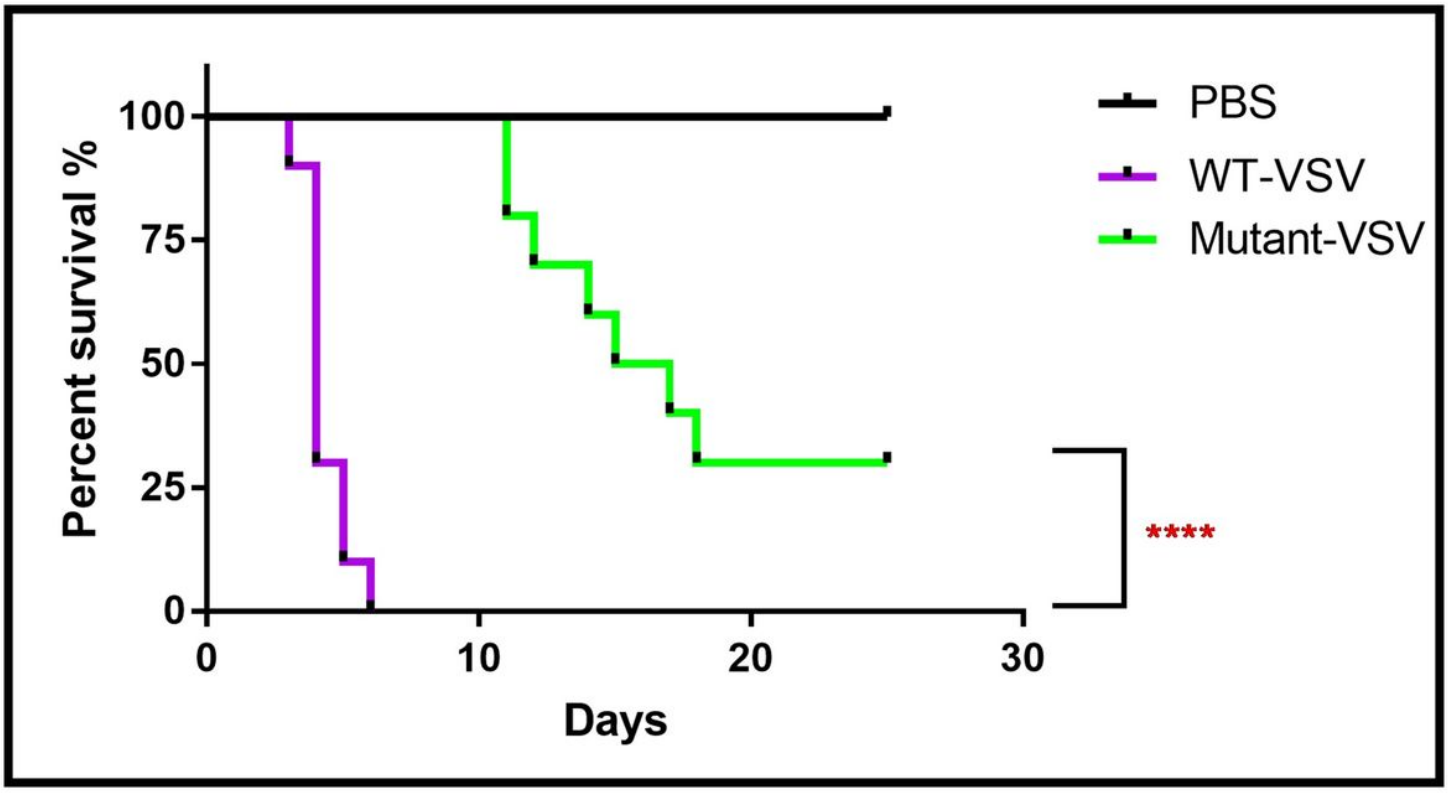

Figure 5

Survival rate of WT-VSV and Mutant-VSV infected mice. WT-VSV, Mutant-VSV and PBS were injected intracranially into the DG domain of adult mice. WT-VSV was rapidly lethal within 1 week and more than half of all deaths occured at 4 DPI, which occured at 14 DPI in Mutant-VSV group. The percent survival was analyzed by Log-rank test (n=10 in each group; $P < 0.0001$). *$P < 0.05$, **$P < 0.01$, ***$P < 0.001$, ****$P < 0.0001$.

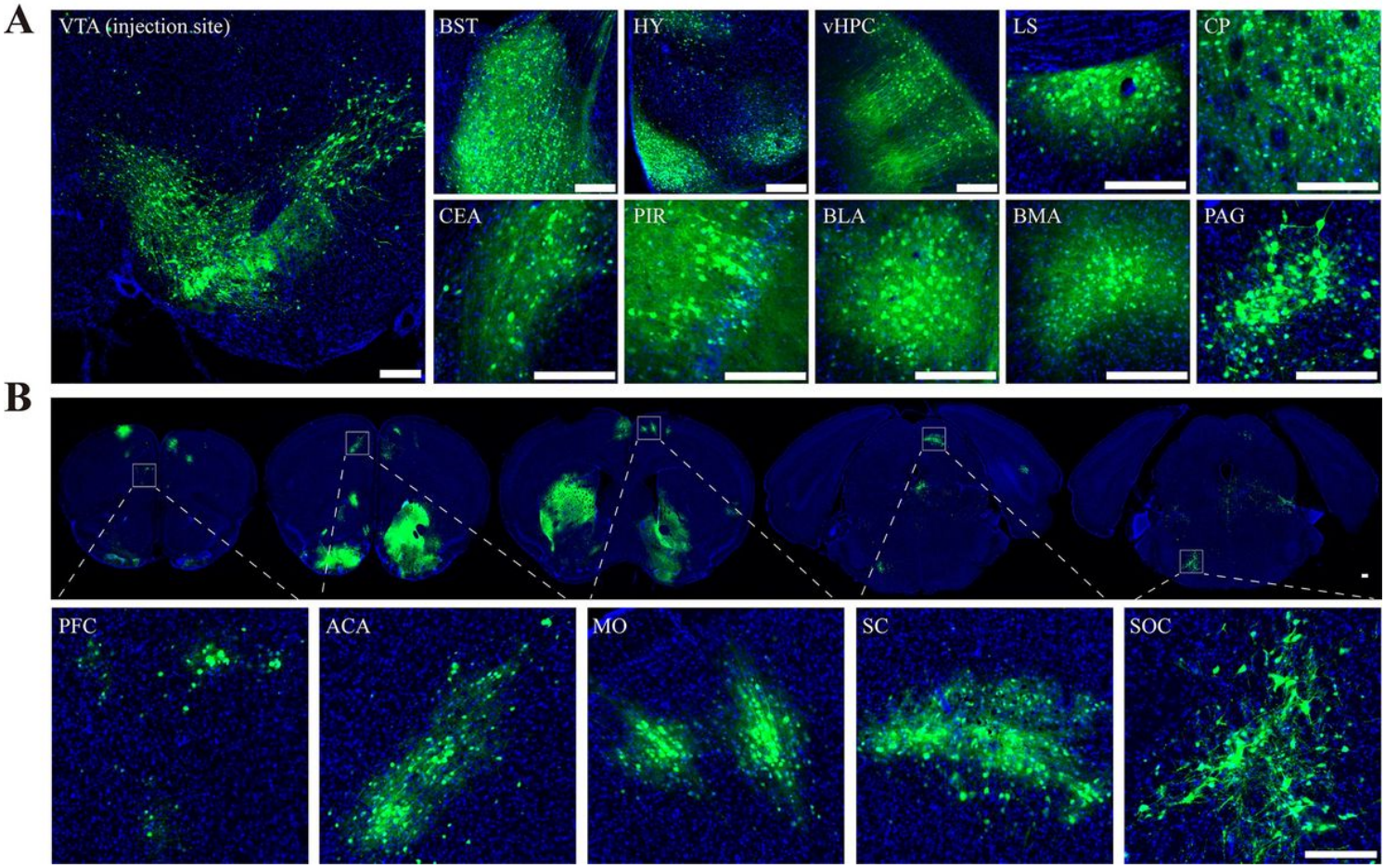

Figure 6

Efficiency of Mutant-VSV in tracing VTA output pathway at 10 days post infection. (A) Normal cell morphology of labeled VTA output neurons can be observed at 10 DPI by using Mutant-VSV. Mutant-VSV were injected into the VTA of C57BL/6 mice, and the brain slices were imaged at 10 days post-injection. (B) More connected downstream brain regions can be revealed through Mutant-VSV. HY: Hypothalamus; vHPC: ventral hippocampus; BLA: Basolateral amygdalar nucleus; PFC: Prefrontal cortex; ACA: Anterior cingulate area; MO: Somatomotor areas; SC: Superior colliculus; SOC: Superior olivary complex. Scale bars =200 μm for A and B.